Manuscript File

Click here to view linked References

Assessing the value of air stagnation indices to reproduce PM_{10} variability in Europe

Jose M. Garrido-Perez[1,2], Ricardo García-Herrera[1,2], Carlos Ordóñez[1]

[1]Dpto. Física de la Tierra y Astrofísica, Universidad Complutense de Madrid, Madrid, Spain.

[2]Instituto de Geociencias (IGEO), CSIC-UCM, Madrid, Spain

Corresponding author: (josgarri@ucm.es)

Abstract

Different air stagnation indices (ASIs) have been proposed to measure the atmospheric diffusion conditions. This paper undertakes a comparative analysis of three ASIs and explores their ability to capture the conditions conducive to elevated PM_{10} (particulate matter ≤ 10 μm) at 306 background sites in Europe for the winter and summer months of 2000–2012. Despite the similar spatial patterns of stagnation frequency found for the three ASIs, the use of different meteorological variables to characterize the dilution capacity of the atmosphere (wind speeds at 10 m and 500 hPa, boundary layer height and ventilation in the boundary layer) leads to important differences in the seasonal cycles. Moreover, the response of the PM_{10} concentrations to stagnation varies with the ASI. Winter PM_{10} anomalies under stagnant conditions are of the same order of magnitude (on average 17.2 to 18.6 μg m^{-3}, around 60 % of the mean values) for the three ASIs. The anomalies are considerably smaller (3.8–5.7 μg m^{-3}, around 19–28 %) in summer, when one of the indices outperforms the others at most locations. The dependence of the PM_{10} concentrations on the ASI components is also evaluated by using correlations and generalized additive models. The results indicate that the consideration of the large-scale circulation is particularly relevant in summer, explaining the different ASI performances during this season. We have also identified some potential improvements that could be made to two of the ASIs. Nevertheless, since the three ASIs are based on fixed thresholds, they cannot deal with non-linear relationships, which limits their ability to explain PM_{10} variability.

Keywords: PM_{10}; Air stagnation; Air pollution; Meteorology; Generalized additive model

1. Introduction

Particulate matter (PM) is one of the main pollutants related to health impacts and impaired visibility (Hyslop, 2009; Anderson et al., 2012; REVIHAAP, 2013; Mukherjee and Agrawal, 2017). Despite the reduction in anthropogenic emissions of PM and its precursors in Europe (Barmpadimos et al., 2012; Guerreiro et al., 2014) and the United States (Cohen et al., 2017; McClure and Jaffe, 2018) over the last decades as a result of the implementation of air quality legislation, the atmospheric concentrations of PM remain worrisome. In Europe, more than 400,000 premature deaths have been attributed to this pollutant during 2016 (EEA, 2019). PM is made up of organic and inorganic particles floating in the air with different morphology and chemical composition. In general, the smaller the size of the particle, the longer its residence time in the atmosphere and the greater the impact on human health (e.g. Fuzzi et al., 2015). Therefore, for air quality regulatory purposes, PM is often classified in two groups, $PM_{2.5}$ and PM_{10}, based on the aerodynamic diameter of the particles (up to 2.5 and 10 μm, respectively) (e.g. EU, 2008). $PM_{2.5}$ is mainly composed of primary combustion particles as well as secondary inorganic and organic aerosols, whereas PM_{10} also includes larger particles like dust, pollen or marine aerosols (e.g. Putaud et al., 2010). Since each component comes from diverse sources and undergoes a number of processes in the atmosphere, unlike most other air pollutants, PM cannot be characterized by the variability of a single compound. Consequently, PM concentrations are particularly difficult to predict.

In the last few years, several indices have been developed in the literature to track the meteorological conditions conducive to enhanced pollution, especially for PM (Horton et al., 2012, 2014; Wang et al., 2016, 2018; Cai et al., 2017; Huang et al., 2017, 2018; Zou et al., 2017). This state of the atmosphere, usually known as air stagnation, is characterized by stable weather, weak winds within the lower troposphere and lack of rainfall. These conditions minimize the horizontal dispersion and vertical mixing of air masses as well as the scavenging of pollutants, favouring their accumulation in the lower atmospheric layers (e.g. Jacob and Winner, 2009; Dawson et al., 2014). Air stagnation indices (ASIs) are usually determined by using predefined thresholds for daily meteorological fields, but each ASI uses different metrics. The most commonly used ASI is that proposed by Horton et al. (2012, 2014) (hereafter, referred to as HO_ASI), following previous work by Wang and Angell (1999). HO_ASI has the advantage that it is based on three fields – 10 m and 500 hPa wind speed and precipitation – which are provided by most meteorological reanalyses and climate models. In a previous paper we have shown that reanalysis and observations compare well when computing this index for Europe (Garrido-Pérez et al., 2018). However, this index presents some limitations to assess the impact of meteorology on air quality (Kerr and Waugh, 2018; Garrido-Perez et al., 2019). Other studies have discussed the adequacy of the 500 hPa wind speed to determine stagnant days under certain conditions. For instance, Dawson et al. (2014) claimed that this criterion is mainly relevant for multiday warm weather stagnation episodes, while Huang et al. (2017) adapted it to account for the influence of the orography in China.

In order to address some of the limitations of HO_ASI, Wang et al. (2016, 2018) and Huang et al. (2018) have proposed alternative ASIs (referred to as WA_ASI and HU_ASI, respectively, from now on) specifically adapted to PM and with a potential to be applied worldwide. Wang et al (2016, 2018) excluded the 500 hPa wind speed condition and used the atmospheric boundary layer height to characterize the vertical mixing of pollutants. Huang et al. (2018) replaced both 10 m and 500 hPa wind speed fields by the ventilation in the boundary layer, and added an extra condition based on the

convective available potential energy (CAPE) and the convective inhibition (CIN) to consider the latent instability of the lower atmosphere. Other indices such as those developed by Cai et al. (2017) and Zou et al. (2017) also describe the transport and dispersion capacity of the atmosphere, but their applicability to different areas of the globe is limited. While the former includes information on circulation patterns which are specific to China, the latter considers spatial averages of meteorological fields over the same region.

In Europe, the spatiotemporal variability of stagnation and its impact on PM have been assessed separately for HO_ASI (Garrido-Perez et al., 2018) and WA_ASI (Wang et al., 2018). However, to the best of our knowledge, no systematic comparison of the three ASIs has been carried out yet for this region. Hence, it is unclear which ASI best fits the European climate and orography. Furthermore, some uncertainty exists about the most appropriate stagnation variables to include in the definition of an ASI, since the dependence of the PM concentrations on meteorology is complex and only a few observational studies are available at the continental scale in Europe. As an illustration, Barmpadimos et al. (2012) constructed generalized additive models at seven background stations in five European countries, finding the boundary layer height, wind speed, wind direction, temperature, precipitation and synoptic weather pattern as the most important meteorological factors affecting PM concentrations. Garrido-Perez et al. (2017) showed that winter PM responds differently to the location of anticyclonic systems. According to that study, the collapse of the boundary layer as well as the reduced wind speeds and rainfall during high-latitude blocking events lead to positive PM anomalies over central Europe. Conversely, enhanced zonal flow, boundary layer growth and increase in the occurrence of precipitation on the northern flank of subtropical ridges reduce PM concentrations over the same region. Other studies have also examined similar dependencies at local or regional scales (e.g. Gietl and Klemm, 2009; Sfetsos and Vlachogiannis, 2010; Barmpadimos et al., 2011; Pateraki et al., 2012; Dimitriou, 2015), but they mainly focus on standard meteorological variables and overlook some of the stagnation components included in existing ASIs.

Consequently, the aims of this study are: (i) to carry out a systematic comparison of three ASIs (HO_ASI, WA_ASI and HU_ASI) and quantify the response of PM concentrations in Europe to stagnation for the three indices, and (ii) to identify the most important meteorological variables related to stagnation that explain PM variability in Europe. For this second objective, we examine correlations of PM with the different ASI components and build statistical models where those meteorological fields are used to reproduce the day-to-day variability of PM. Note that, despite the existence of indices that provide information about the intensity of air stagnation (Feng et al., 2018) or which combine stagnation intensity with emission information (Feng et al., 2020), this work deals with indices that are related to the frequency of stagnation. To get a seasonal perspective of potential variations in the PM–stagnation relationships, we conduct separate analyses for winter (December, January, February; DJF) and summer (June, July, August; JJA) during a 13-year period. We have opted to use PM_{10} instead of $PM_{2.5}$ observations due to the better data availability for the former in Europe.

The paper is structured as follows. Section 2 introduces the area of study, PM_{10} observations, ASIs and meteorological data. Section 3 presents the potential explanatory drivers of PM_{10} and describes a statistical model used to diagnose the strength of their relationships with PM_{10}. Section 4 compares the spatiotemporal patterns of air stagnation and the relationship with the PM_{10} concentrations over Europe for the three ASIs. Section

5 presents the results of the statistical model. Finally, Sections 6 and 7 discuss and summarize the main findings of this work.

2. Data

2.1. Area of study

Europe is a climatically diverse continent. The differences among European regional climates are mainly due to the complex orography of the continent and the great atmospheric variability that characterizes mid-latitudinal regions. The area of study comprises western Europe, central Europe and part of eastern Europe (Figure S1). This region includes a large portion of the Great European Plain, stretching from the Pyrenees and the French Atlantic coast in the west to the Russian Ural Mountains in the east, as well as plateaus and mountain ranges in the Alpine region and the southern half of the continent. Accordingly, air stagnation has considerable spatial heterogeneity over the region.

Garrido-Perez et al. (2018) identified five subregions where stagnation shows coherent spatiotemporal patterns. Central and eastern Europe, which are characterized by cold winters and relatively warm summers, present moderate frequency and small interannual variability of stagnation. The northern regions are affected by strong surface winds and ample precipitation, presenting low frequency and seasonal variability in stagnation compared to the southern regions, where the highest frequency of stagnation occurs. As the Mediterranean area is often under the influence of subtropical high-pressure ridges, the climate of this region is mostly characterized by low precipitation, calm winds and elevated temperatures compared to the rest of the continent (García-Herrera and Barriopedro, 2018). In fact, Mediterranean Europe is expected to be one of the mid-latitudinal regions most affected by air stagnation by the late twenty-first century if emissions of greenhouse gases are not reduced (Horton et al., 2012, 2014).

2.2. PM_{10} observations

We have used daily average PM_{10} concentrations during the period 2000–2012 extracted from the European Environment Agency's air quality database (AirBase) (http://www.eea.europa.eu/data-and-maps/data/airbase-the-european-airquality-database-8, last access: July 2020). These data have recently been employed by several studies to understand the influence of large-scale circulation on PM_{10} in Europe (Garrido-Perez et al., 2017; Ordóñez et al., 2019). In this work, only the stations catalogued as background with at least 75% of the data available separately during the summer and winter months of the period of analysis have been considered. Although most of the resulting 306 sites are located in France (37.3%), Germany (27.5%), the Czech Republic (9.2%) and Switzerland (4.6%), they cover 18 different European countries. Figure S1 illustrates the seasonal means of PM_{10} at each location. The average over all sites ranges from 20.5 μg m^{-3} in summer to 28.6 μg m^{-3} in winter, but there are considerable regional differences. The highest concentrations are found for eastern Europe, northern Italy and some sites in the Iberian Peninsula, where the winter averages exceed 40 μg m^{-3}. Winter mean concentrations of ~30 μg m^{-3} are also common to many sites in Benelux, southeastern France, Switzerland and southern Germany, whereas they are lower over other regions. Similar patterns, although with lower concentrations, are found in summer. Here we present results for the observed raw concentrations. Additional analyses based on detrended PM_{10} time series indicate that the results are not very sensitive to the changes in anthropogenic emissions during the 13-year period (not shown).

2.3. Air stagnation indices and meteorological data

We have used these ASIs: HO_ASI (Horton et al., 2012, 2014), WA_ASI (Wang et al., 2016, 2018) and HU_ASI (Huang et al., 2018). The three indices are based on predefined thresholds of daily meteorological fields and are binary, i.e. they can only take two values (stagnant/non-stagnant). HO_ASI considers that a location is stagnant on a given day if three conditions are simultaneously met: daily average wind speed at 10 m (Wsp10) below 3.2 m/s, daily average wind speed at 500 hPa (Wsp500) below 13.0 m/s and daily accumulated precipitation (Prec) below 1 mm (i.e. dry day).

WA_ASI requires that Prec is below 1 mm and that the daily boundary layer height (BLH) is below a threshold that depends on the Wsp10 field and the season, following equations 1–4:

Spring: $BLH = 3.57 * 103 * \exp(-3.35 * Wsp10) + 0.352$ (1)

Summer: $BLH = 7.66 * 10 * \exp(-2.12 * Wsp10) + 0.443$ (2)

Autumn: $BLH = 1.88 * 104 * \exp(-5.15 * Wsp10) + 0.440$ (3)

Winter: $BLH = 0.759 * \exp(-0.6 * Wsp10) + 0.264$ (4)

These equations have been derived by fitting Wps10 and BLH on dry days with normalized PM concentrations close to 100% at sites distributed throughout China, the United States and Europe (for more detail see Wang et al., 2018).

HU_ASI considers a location as stagnant if three conditions are met on a given day. First, Prec must be below 1 mm. Second, daily maximum ventilation (Vent), defined as the integral of the horizontal wind speed within the boundary layer (see equation 5), must be below 6000 m^2/s.

$$Vent = \int_0^{BLH} Wsp(z)\, dz \quad (5)$$

Where

z is the height above the surface

Wsp(z) is the wind speed at a height of z.

Finally, this index uses two thermodynamic parameters, CAPE and CIN, to provide additional information on the strength of atmospheric convection in some areas of the original region of study, i.e. China. According to Huang et al. (2018), stagnation can only occur if the value of CAPE is below that of CIN. We have adapted that condition to Europe, following the work by Taszarek et al. (2018). Consequently, here the occurrence of stagnation excludes potential thunderstorm days (PTDs), i.e. those with CAPE > 100 J/kg and CIN > -50 J/kg. Summarizing, our adaptation of the index by Huang et al. (2018) for Europe considers that there is stagnation if there is a dry day (Prec < 1 mm), Vent < 6000 m^2/s and there is no potential thunderstorm day (non-PTD).

The meteorological fields required to compute the ASIs – wind speeds at different heights, Prec, BLH, CAPE and CIN - have been obtained from the ERA5 reanalysis product (Hersbach et al., 2020) at 0.75º × 0.75º horizontal resolution for the 1981–2012

period. Even though we analyse the relationships of the ASIs with PM_{10} concentrations during a shorter 13-year period (2000–2012), we use 30 years of reanalysis data (1981–2010) to extract robust climatological features of the ASIs over the region of study. Daily mean sea level pressure (SLP), 500 hPa geopotential height (Z500), 2m temperature and 1000 hPa relative humidity have also been employed as potential drivers of PM_{10} day-to-day variability (see next section). Daily precipitation has been computed as the sum of 1-h accumulated precipitation forecast for twenty-four time intervals on each day. Daily averages of wind speed, SLP, Z500, temperature at 2m and relative humidity have been calculated by averaging four analysis values at the standard meteorological hours 00, 06, 12 and 18 for each day. While the daily values of BLH, CAPE and CIN correspond to those at 12 UTC, daily maximum ventilation is computed as the highest value at the standard meteorological hours 00, 06, 12 and 18.

Daily time series and maps of the three ASIs over Europe, based on ERA5 data, have been made available at http://147.96.21.169/ for use in future atmospheric and air quality studies. This is the first publicly available dataset of air stagnation in Europe.

3. Statistical method

3.1. Statistical model

Generalized Additive Models (GAMs) are effective tools to conduct non-linear regression analysis of air pollutant time series (Dominici et al., 2002; Barmpadimos et al. 2011, 2012; Boleti et al., 2018; Ordóñez et al., 2020). They are semi-parametric extensions of the generalized linear model that assume that there is an additive effect of the predictors on the predictant. We have applied this statistical technique, provided by the pyGAM Python module (Servén and Brummitt, 2018), to each station and season separately in order to explore the relationships between the PM_{10} concentrations and a pool of potential meteorological drivers. Factor and spline smoothing functions have been used to model the pollutant response to categorical and continuous variables, respectively. The factor function fixes constant values for each categorical attribute, while the spline function constructs the response curve from several polynomial segments that connect smoothly at their joints. In particular, we have used a regression spline known as penalized B-spline or P-spline. This technique imposes smoothness by directly penalizing the differences between adjacent coefficients, avoiding overfitting. Model fitting is achieved by maximum likelihood estimation. Details can be found in Wood (2006) and references therein. In addition, it is well known that PM concentrations follow a lognormal distribution (Bencala and Seinfeld, 1976). Therefore, like Barmpadimos et al. (2011, 2012), we have used the log-transformed daily concentrations of PM_{10} in order to achieve normally distributed residuals and improve the homoscedasticity of the model. The general form of the model used in this work is as follows:

$$\log(PM_{10}) = \beta_0 + \sum_x s_x(A_x) + \sum_y f_y(B_y) \quad (6)$$

where

β_0: intercept of the model

$s_x(A_x)$: smoothing spline function on continuous feature A_x

$f_y(B_y)$: factor function on categorical feature B_y

While PM concentrations show a complex dependence on the meteorology (e.g. Tai et al., 2010, 2012), initially we have only considered potential explanatory variables that are related to stagnation. Wsp10, Wsp500, Vent, BLH and the transport wind speed (Twsp) have been included as indices of atmospheric horizontal dispersion capability and vertical mixing. Note that all of them, except for Twsp, are required to compute at least one of the three ASIs. Twsp is a parameter that takes into account Vent and BLH simultaneously (Twsp = Vent/BLH) to measure the average strength of horizontal dilution within the boundary layer (Huang et al., 2018). Moreover, the occurrences of dry days (Prec < 1 mm) and non-PTDs are also incorporated to consider the wet deposition of pollutants as well as the real latent instability of the lower troposphere, respectively. Unlike the other explanatory variables, which are continuous, these two fields are binary. We have also included Z500 and SLP among the potential drivers to account for synoptically-driven variability of PM_{10} in Europe (Garrido-Perez et al., 2017; Ordóñez et al., 2019).

3.2. Screening regression

A stepwise procedure has been used for the selection of the best set of predictors from the pool of meteorological variables described above. The algorithm is similar to that applied in previous studies to model the atmospheric concentrations of the hydroxyl radical, PM or ozone (Jackson et al., 2009; Barmpadimos et al., 2011; Otero et al., 2016). It consists of the following five steps: 1) We evaluate the strength of the regression between the pollutant and each of the potential predictors. The explanatory variable with the highest deviance explained by the GAM is selected. 2) We recompute the GAMs using each of the remaining potential predictors separately together with the previously selected variable. The combination with the highest deviance explained is considered as the pool of selected variables. 3) We check the choice from the first step. The variable selected in that step is ignored and each of the remaining potential predictors are separately added to the model together with the variable selected in the second step. If any of these combinations performs better than that of the second step, then it is considered as the new pool of selected variables. 4) We test the collinearity between the selected variables to avoid redundancy and oversensitivity of the model to the data. For that purpose, we have computed the Variance Inflation Factor (VIF; Freund and Wilson, 1998) for each pair of selected variables. Following Barmpadimos et al. (2011), if VIF exceeds 2.5 for a pair of predictors, the collinear variable with the smallest contribution is excluded from the screening process. This threshold is quite restrictive compared to the values used by other analyses (e.g. VIF=10 in Otero et al., 2016), restricting the collinearity of the variables included in the model. 5) The procedure is repeated from steps 2 to 4 until the inclusion of a new variable in the pool of selected predictors results in an increase of the deviance explained below one percent or if all the potential explanatory variables have already been selected.

Once the GAM has been fit for a given location and season, we have used partial dependence plots (PDP) to further explore the dependence of the PM_{10} concentrations on their drivers (Friedman, 2001). These plots are graphical representations of the marginal effect that the explanatory variables included in the model have on PM_{10}, accounting for the average effects of all other predictors. This helps understand the importance of each feature in the model and illustrates how PM_{10} concentrations vary when a driver changes, showing if their relationship is linear or more complex.

4. Comparison of ASIs

We have first compared the spatiotemporal variability of air stagnation frequency over Europe for the three different ASIs. Figure 1 shows the annual average percentage of air stagnation days (%) for each of these indices. The spatial patterns share some common features, with considerable spatial heterogeneity across Europe. The highest stagnation frequency occurs over the Mediterranean area, whereas the lowest stagnation centres are located at higher latitudes, specifically over the British Isles, northwestern France, Benelux, northern Germany, Denmark, Poland and the Baltic states. These spatial patterns resemble those of the average number of events (defined as the sequence of one or more consecutive stagnation days) per year and the average event duration (Figure S2). However, the absolute values and the seasonal cycles differ among the ASIs. HO_ASI is characterized by a winter minimum and a summer maximum, whereas the opposite occurs for HU_ASI, as seen in Figure S3 and also reported by Huang et al. (2018) for China. On the other hand, WA_ASI presents the smallest seasonal dependence.

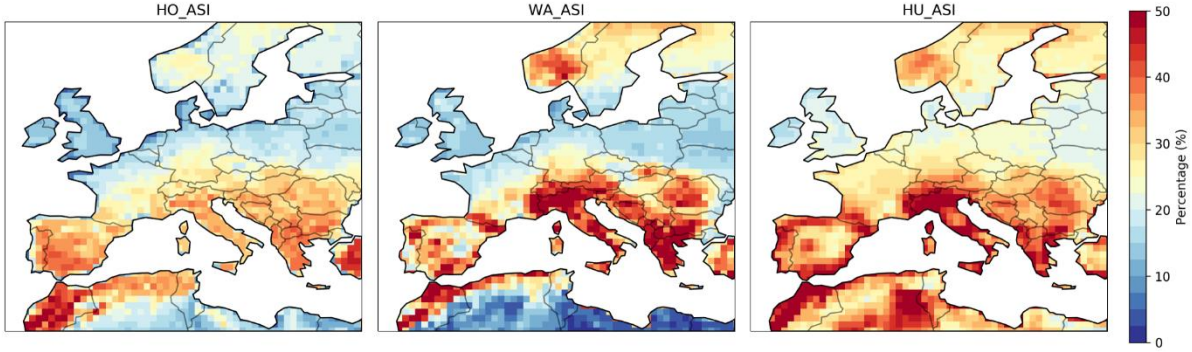

Figure 1. Annual average percentage of stagnation days (%) during the period 1981–2010 for HO_ASI (left), WA_ASI (middle) and HU_ASI (right).

The differences in the temporal variability of stagnation among ASIs must be attributable to the distinct conditions used in the definition of each index. Therefore, we have examined how often stagnation conditions are met separately for each component (Figure 2). First, the occurrence of dry days (top panels) exceeds 50% for most of the study area and increases gradually as latitude decreases to around 80% at some locations of southern Europe, explaining to a certain extent the north-south gradient in stagnation. The use of this precipitation condition as an indicator of the washout of pollutants is common to all indices, but the approaches to characterize the atmospheric horizontal dispersion capability and vertical mixing are different. HO_ASI uses two wind speed conditions at 10 m (Figure 2d) and 500 hPa (Figure 2g). The former condition presents considerable regional heterogeneity, with spatial patterns that closely resemble those of the frequency of stagnation over most regions, indicating the relevance of this meteorological variable. However, the 500 hPa wind speed might be the limiting factor in the occurrence of stagnation over large parts of Europe since it fulfils the stagnation conditions less frequently than the rest of components over most regions. Anyway, both wind speed conditions are more/less likely to be met in summer/winter due to the weak/strong climatological winds in these seasons (Figures S4 and S5), explaining the seasonality of this ASI. Note also that Wsp500 is a rather smooth field because it is hardly influenced by processes in the boundary layer. As a consequence, the frequency of stagnation is more spatially uniform for HO_ASI than for the other two indices over some regions such as the Iberian Peninsula and Scandinavia (Figure 1).

As mentioned above, the seasonal cycle is reversed in the case of HU_ASI as compared to HO_ASI. The reason lies in the dependence of Vent on BLH (see equation 5), which maximizes in summer and minimizes in winter (Figure S6). This implies that the Vent condition, whose spatial pattern (Figure 2f) resembles to some extent that of the 10 m wind speed condition of HO_ASI (Figure 2d), is more likely to be met in winter than in summer (Figure S7), leading to a seasonal cycle of HU_ASI characterized by a maximum in winter and a minimum in summer. Note that the occurrence of PTDs does not limit that of stagnation since they are highly unusual (Figure 2h). This condition is mainly relevant over some regions in summer (not shown). On the other hand, WA_ASI is defined based on a Wsp10-BLH condition which shows similar spatial patterns to those of the Vent condition and, to a lesser extent, those of Wsp10 (Figure 2d-f). However, the Wsp10-BLH condition is less often met than the Vent condition of HU_ASI over the British Isles and the Great European Plain, resulting in somewhat lower stagnation frequency for WA_ASI in those regions (Figure 1). Finally, the inter-seasonal variability of stagnation is considerably smaller for this index than for the rest of ASIs, because of the season-specific formulation used to construct the Wsp10-BLH condition (Eqs. 1–4).

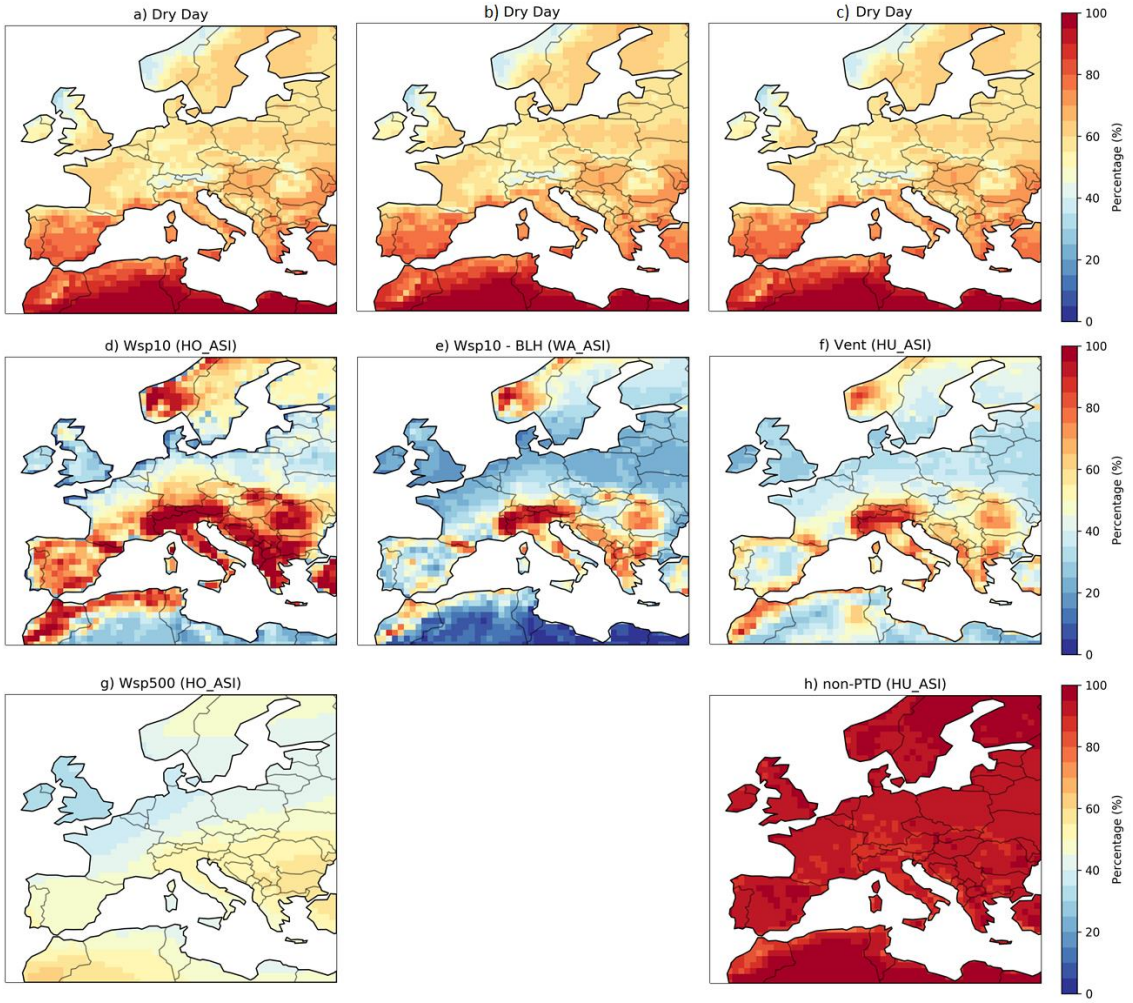

Figure 2. Annual percentage of days that fulfil stagnation conditions for the different components of HO_ASI (a,d,g), WA_ASI (b,e) and HU_ASI (c,f,h) during the period 1981–2010. Full details of these conditions are given in Section 2.3.

Next, we examine the dependence of PM_{10} on each ASI by computing PM_{10} anomalies as the differences of the mean concentrations between days with and without stagnation at each site. This has been done separately for winter and summer. Winter (top)

and summer (bottom) PM_{10} anomalies are shown in Figure 3 when they are statistically significant at the 95% confidence level (two-tailed t-test). As expected, stagnation enhances the PM_{10} concentrations at all sites in winter, but its impact is small over some regions in summer. The strongest effect is found over Benelux and the inner part of the continent (including eastern France, Switzerland, the southern half Germany, the Czech Republic and Poland) for both seasons. The lowest anomalies are located over western and central France, Spain and northern Germany, as well as in Italy during summer. The magnitude of these anomalies also varies with the ASI. In winter, the response of PM_{10} to stagnation is quite similar among the three indices, with average concentration anomalies between 17.2 and 18.6 μg m^{-3}. This corresponds to ~60% of the seasonal mean concentrations (see top panels of Figure S8, where PM_{10} anomalies have been normalized by the seasonal mean concentrations at each location). Moreover, there are anomalies over 25 μg m^{-3} at some locations for all indices. In summer, HO_ASI shows the largest PM_{10} anomalies, with an average of 5.7 μg m^{-3} compared with 4.6 and 3.8 μg m^{-3} for WA_ASI and HU_ASI, respectively. While this difference may seem small in absolute terms, it still represents a considerable portion of the seasonal mean (see Figure S8, bottom panels). The average normalized anomalies increase from 19 and 22 % for HU_ASI and WA_ASI, respectively, to 28 % for HO_ASI, confirming the higher specificity of the latter in this season. Nevertheless, these anomalies are less than half of those found in winter for all indices.

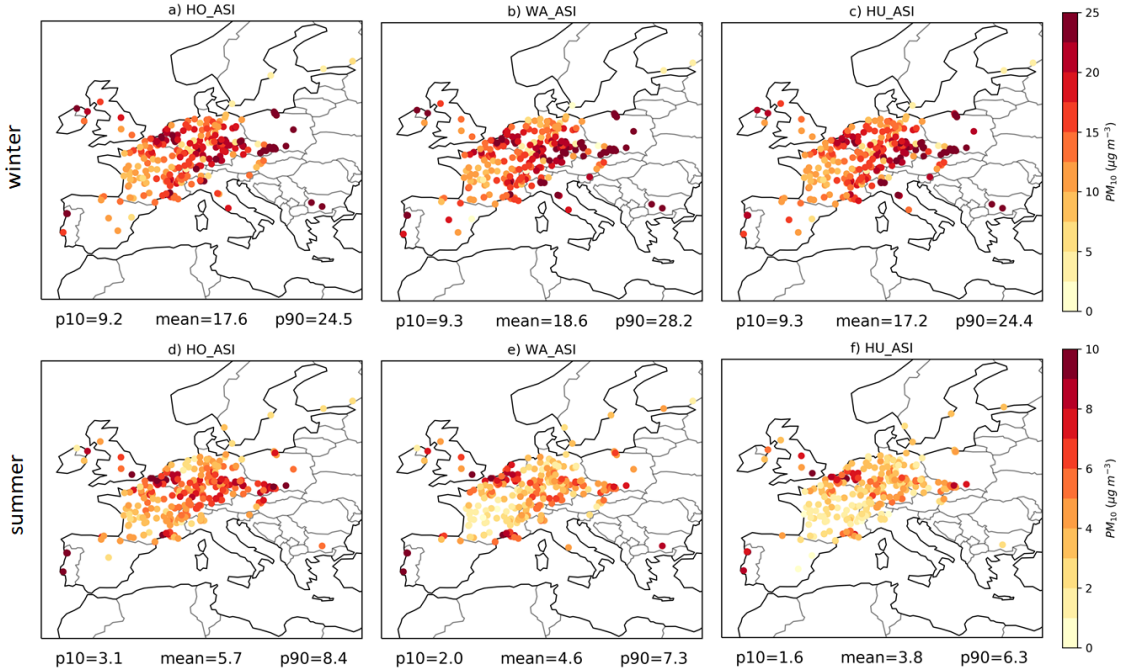

Figure 3. Composites of winter (top) and summer (bottom) PM_{10} concentration anomalies (μg m^{-3}) on days with stagnation with respect to days without stagnation for HO_ASI (left), WA_ASI (middle) and HU_ASI (right) during the period 2000–2012. Anomalies are only shown when they are statistically significant at the 95% (determined through a two-tailed t-test). Note the differences in the colour scales, indicating considerably higher anomalies in winter than in summer. The numbers below the panels respectively indicate the 10th percentile (p10), mean and 90th percentile (p90) across all sites.

We have also identified the ASI yielding the highest PM_{10} anomaly at each location (Figure 4). In winter, WA_ASI outperforms the other indices for almost half of

the sites (137), whereas HO_ASI and HU_ASI are selected for 103 and 66 sites, respectively. Nevertheless, no clear spatial patterns have been identified as the ASI selection seems to be more specific to the local settings of the stations than to the geographical regions, with the exception of some relatively small regional clusters (e.g. HU_ASI tends to be selected in some areas of northern Germany and western Austria). Conversely, HO_ASI is associated with the highest PM_{10} anomalies in summer at 263 sites, compared to only 43 sites for the other two ASIs. While HO_ASI clearly beats the other two indices over most of the continent in summer, WA_ASI performs best at coastal sites.

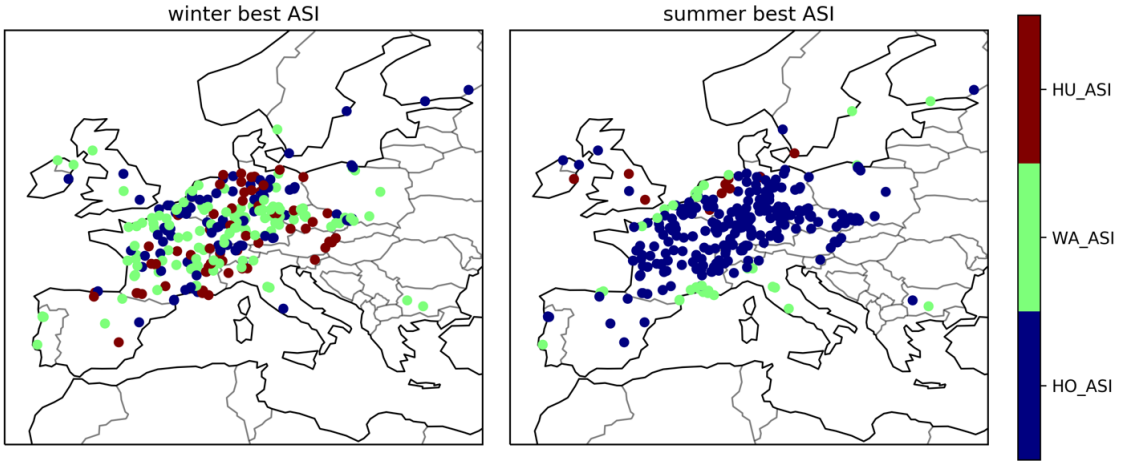

Figure 4. Spatial distribution of the ASIs with the highest PM_{10} anomalies in Figure 3.

The previous results indicate that the relationships between each ASI and the PM_{10} concentrations vary with location and season. Therefore, a more detailed assessment of the impact of each stagnation component on this pollutant is required to better understand the spatiotemporal responses of PM_{10} to each ASI. In order to do so, we have computed Spearman's rank correlation coefficients between the daily time series of PM_{10} concentrations and the daily values of Wsp10, Wsp500, Vent, BLH and Twsp. Only these meteorological variables have been considered in this analysis because the characterization of the atmospheric dilution capacity is the main difference among the three ASIs. Note also that Spearman's correlation measures the strength of monotonic relationships (whether linear or not) between variables. Figure 5 shows the first, second and third most correlated variables with PM_{10} in winter (top) and summer (bottom). In winter, Vent and Wsp10 are the fields that best explain the day-today variability of PM_{10}, besides BLH in some parts of northern Europe. Moreover, Twsp seems to be a better predictor than Wsp500, as it is often selected as the variable with the second and third best correlations. These results seem to be inconsistent with the fact that the application of HU_ASI yields the lowest winter PM_{10} anomalies on stagnant days (although by a low margin), as it is the only ASI defined based on Vent. In fact, HO_ASI results in slightly higher PM_{10} anomalies than HU_ASI despite the lowest correlations found for Wsp500 in this season. This could be due to non-linear relationships between the meteorological variables and PM_{10} concentrations. Since ASIs are defined based on fixed thresholds, they cannot take this into account as does the Spearman's rank correlation coefficient. We have repeated the analysis shown in Figure 5 but using the Pearson's correlation coefficient, which assesses linear relationships, instead of Spearman (Figure S9). In this case, Wsp10 is the field with the highest correlations at most sites in winter, while the correlations for Vent and Twsp decrease compared to those of other variables, which now

seems consistent with the somewhat smaller PM_{10} anomalies found for HU_ASI than for the other two indices.

More marked spatial patterns are found in summer for both Spearman and Pearson correlation coefficients, with Wsp500 presenting the highest correlations over most of France and Wsp10 in other regions, consistent with the highest PM_{10} anomalies reported for HO_ASI in this season. In addition, BLH has been selected at some of the coastal sites where WA_ASI outperformed the other two indices. Finally, it must be noted that Twsp is the field with the second best correlations at many sites in summer. As expected, unlike winter, this field becomes more relevant than Vent, with the exception of some coastal locations. While subsidence under stagnant clear-sky anticyclonic conditions limits the dilution capacity of the lower atmosphere, yielding the accumulation of pollutants close to the surface, Vent values can still be high because the strong radiative and surface heat fluxes favour the development of the boundary layer over continental areas under such situations in summer. This suggests that replacing the ventilation condition by another one based on an appropriate Twsp threshold in the definition of HU_ASI could improve the performance of the index for Europe in summer.

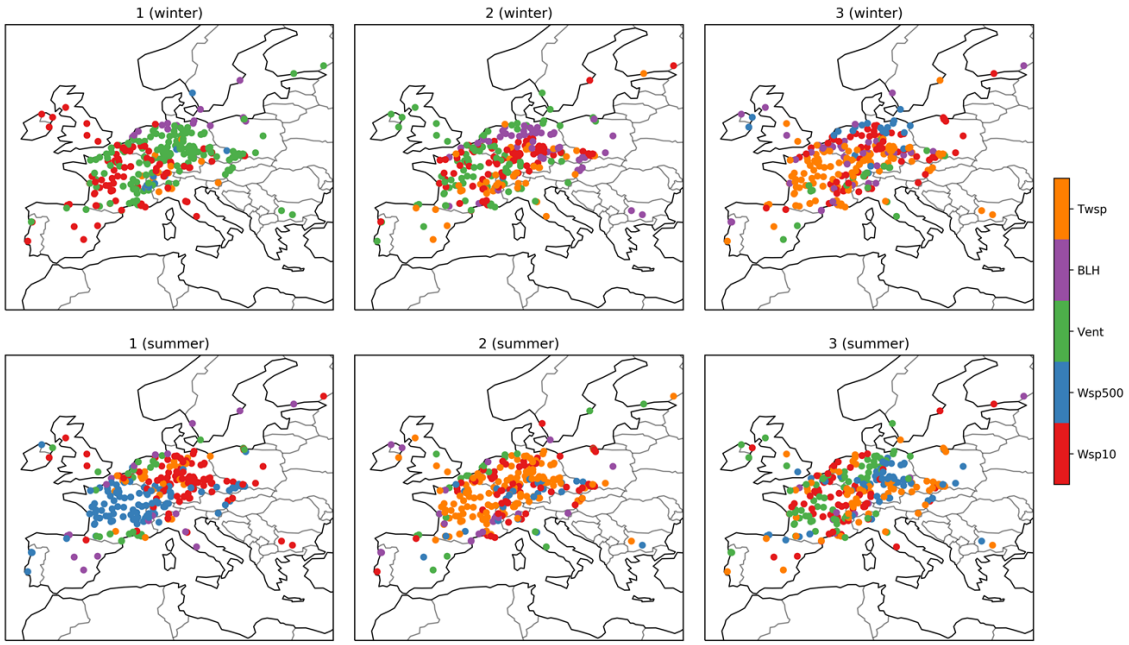

Figure 5. First (left), second (middle) and third (right) most correlated meteorological variables (either positively or negatively) with daily PM_{10} concentrations using the Spearman rank correlation coefficient for all stations in winter (top) and summer (bottom) of 2000–2012.

5. Statistical modelling of daily PM_{10} as a function of stagnation components

None of the three ASIs tested seems to clearly outperform the others all year round when examining PM_{10} anomalies under stagnant vs. non-stagnant days (Figure 4). Moreover, our correlation analyses have raised contrasting responses of the PM_{10} concentrations to some of the ASI components depending on the location and season (Figure 5). While some of those components are expected to show some collinearity, others may have an additive effect on the PM_{10} concentrations. Consequently, we have constructed GAMs to identify the ASI components that drive PM_{10} variability at each location separately for summer and winter. Note that, with the exception of dry day and non-PTD, which are treated as discrete variables, we do not use the threshold exceedance

of the other ASI components but their actual daily values in the models. We also include Z500 and SLP to consider synoptically-driven PM_{10} variability.

First, we have performed a screening analysis as described in Section 3.2. The resulting combinations of explanatory variables are shown in Tables S1 and S2 for winter and summer, respectively. Table 1 also summarizes how often each variable is selected over all sites. The precipitation condition (dry day), which is common to all three ASIs, is the most used predictor in winter and the second least selected one in summer. The other discrete variable, i.e. non-PTD, is selected at only 5% of the sites in winter, as expected, rising to 11% in summer. This indicates a weak relationship with PM_{10} and a low added value of this field as a result of the low frequency of occurrence of PTD in the region of study (Figure 2h).

Table 1. Percentage of sites (out of a total of 306) for which each predictor was selected by the backward stepwise regression in winter and summer.

	Wsp10	**Wsp500**	**Vent**	**BLH**	**Twsp**	**Prec**	**non-PTD**	**Z500**	**SLP**
Winter	43	78	57	31	43	82	5	76	69
Summer	65	85	42	62	30	13	11	100	89

Among the stagnation components that characterize the atmospheric horizontal dispersion and vertical mixing of air masses, Wsp500 is the most used predictor in both seasons. This does not necessarily mean that it is the most important variable in reproducing PM_{10} variability, but that it is the one that best complements the rest of meteorological drivers tested in the model. The moderate selection frequency of Wsp10, Vent, BLH and Twsp is due to their close relationship. Since Vent and Twsp depend on both wind speed and BLH, the inclusion of these fields in the model accounts for both the horizontal and vertical dilution capacity of the atmosphere. Therefore, these four variables are highly correlated and are often removed from the optimal set of predictors to avoid multicollinearity. In fact, their simultaneous inclusion occurs in less than 2% of the stations for both seasons, while any combination of three of them remains below 15%. It is noteworthy the fact that Vent is preferred over Wsp10 and BLH in winter, which is in line with the Spearman's correlations reported in Section 4 (Figure 5) but not with the Pearson's correlations (Figure S9). This suggests that the consideration of non-linear relationships between the variables that characterize the dilution capacity of the atmosphere and PM_{10} concentrations is key to understand the additive contribution of each explanatory variable.

An example of the non-linear dependence of PM_{10} on Vent and other fields at a representative station in southern Germany can be seen in Figure 6. As expected, an increase in Vent results in a decrease of the PM_{10} concentrations, but this trend is much steeper for low values of Vent. The figure also shows that PM_{10} concentrations are enhanced on days with low mid-tropospheric winds and no rain. On the other hand, the relationship between PM_{10} and Z500, with a maximum at around 550 dam, is clearly non-linear. This occurs because the regional response of PM_{10} to anticyclonic systems not only depends on their intensity but also on their position (Garrido-Perez et al., 2017). The evaluation of Z500 and SLP provides information on the relative importance of the synoptic conditions. The selection frequency of these variables is high in both seasons, especially in summer (89% for SLP and 100% for Z500). In addition, their simultaneous inclusion occurs at 51% and 90% of the stations in winter and summer, respectively. This, together with the high selection frequency of Wsp500, suggests that the inclusion of a meteorological variable representing the large-scale flow in the ASI definition is

particularly useful in summer, which is in line with the highest skill of HO_ASI during this season. Wsp500 also seems to be of value in winter, although the 13 m/s threshold used for this field might need to be relaxed because of the strong climatological wind speeds in that season (see Fig. S5).

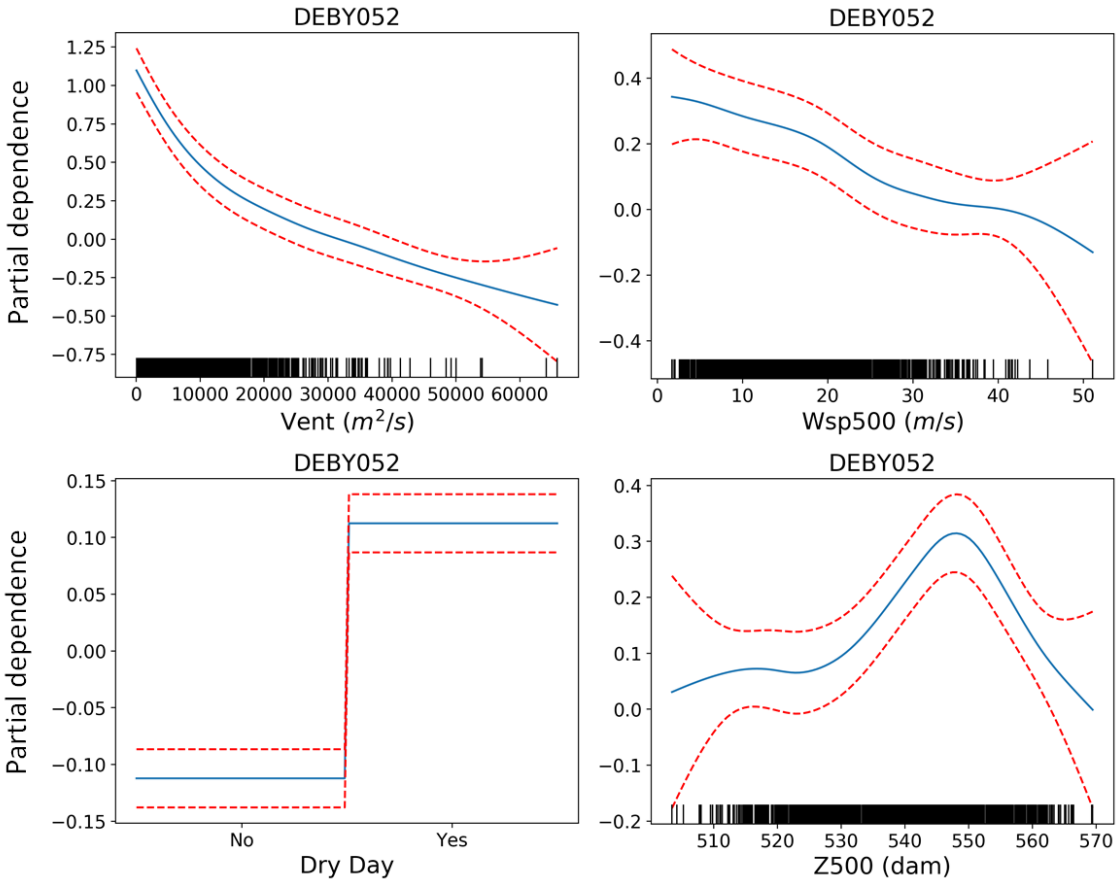

Figure 6. Partial dependence plots of the drivers used in the GAM model for DEBY052 site (Germany, [48.4º N, 10.0º E]) in winter. Red dotted lines indicate the 95% confidence intervals for the estimated functions (blue solid lines). The distribution of the data is indicated by the vertical marks along the x-axis for the continuous variables (rug plot).

Finally, Figure 7 displays the spatial distribution of the deviance explained by the GAMs using the resulting combinations of explanatory variables for winter and summer. The models explain a larger fraction of the day-to-day variability of PM_{10} in the former season, with average deviance explained over all sites ranging from 0.37 in summer to 0.43 in winter. The best performance is found over Benelux and the inner part of the continent, with values up to ~0.6 in winter and ~0.5 in summer at some sites of eastern France, Switzerland, southern Germany and the Czech Republic. These are among the European regions where the PM_{10} concentrations are most influenced by large-scale patterns such as anticyclonic systems or the North Atlantic jet (Garrido-Perez et al., 2017; Ordóñez et al., 2019), indicating the importance of the synoptic conditions to capture inter-daily variations of PM_{10}.

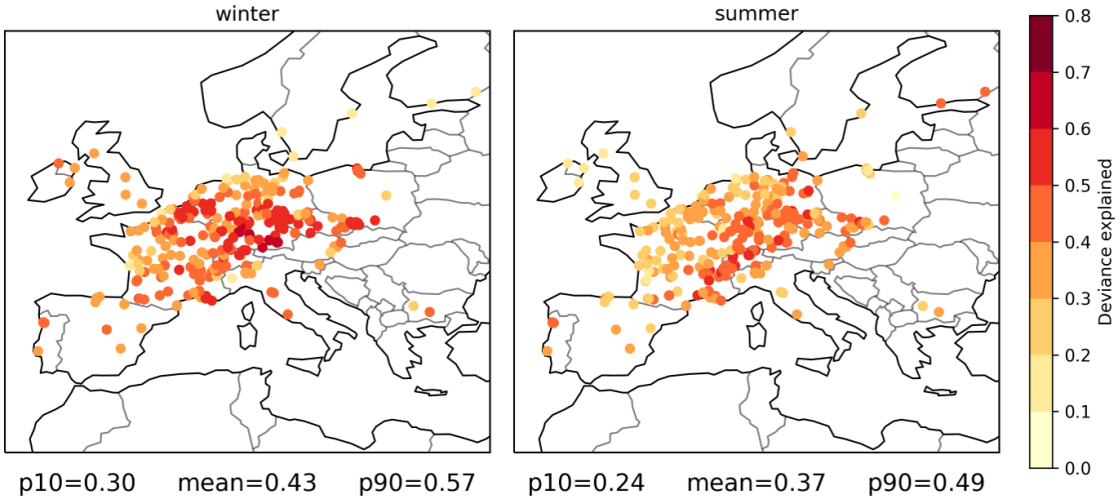

Figure 7. Deviance explained by the GAMs for all stations in winter (left) and summer (right) during the period 2000–2012. The list of variables considered as potential predictors is available in Table 1. The numbers below the panels respectively indicate the 10th percentile (p10), mean and 90th percentile (p90) across all sites.

6. Discussion

The resulting deviance explained by the GAMs is moderate for most locations, ranging from an average of 0.37 in summer to 0.43 in winter (Figure 7). However, there is still room for improvement since we have not considered some meteorological variables and factors that affect PM. For instance, the effect of the persistence (defined as the concentrations of air pollutants on the previous day) is well known from previous studies (e.g. Vlachogianni et al., 2011, for NO_x; Otero et al., 2016, for ozone; Ordóñez et al., 2019, for PM_{10}). Increases in relative humidity are related to wet conditions with reduced suspension of dust (Wise and Comrie, 2005), but also to the formation of ammonium nitrate (Liao et al., 2006; Lecoeur and Seigneur, 2013). Changes in temperature have also been reported to influence PM concentrations showing multiple competing effects. On the one hand, high temperatures increase the rate of SO_2 oxidation and promote the emission of biogenic volatile organic compounds, resulting in enhanced sulphate concentrations and production of secondary organic aerosols, respectively (Dawson et al., 2007; Heald et al., 2008; Jacob and Winner, 2009; Tai et al, 2010). On the other hand, high temperatures lead to the volatilization of ammonium nitrate and semi-volatile organic aerosols, reducing the concentrations of PM (Dawson et al, 2007; Aksoyoglu et al., 2011; Jimenez-Guerrero et al., 2012). In an attempt to consider some of these complex relationships, in addition to the well-known covariation of temperature and humidity with other meteorological variables affecting PM (Tai et al., 2010, 2012), we have rebuilt the GAMs including the persistence, temperature and relative humidity among the potential explanatory variables.

The deviance explained by the new models rises to an average of 0.66 in winter and 0.60 in summer, exceeding 0.80 at some locations of central Europe in the former season (Figure 8). This is a considerable improvement compared to the values reported for the same seasons in Figure 7. Persistence is selected for all sites both in winter and in summer, temperature is respectively chosen at 74% and 49% of the sites in winter and summer, and relative humidity at 72% and 54% of the sites in the same seasons. Furthermore, if persistence was the only new field added to the pool of potential

predictors, the average deviance explained would be 0.60 for both seasons. While we have not quantified the changes in the collinearity of the predictors for the different models, the results provide evidence for the strong effect of persistence compared to that of temperature and relative humidity. Overall, the use of the persistence together with meteorological fields related to stagnation suffices to obtain explained deviances of ~0.60 in both seasons, while the inclusion of other fields such as temperature and relative humidity contributes to raising those values in winter but not in summer.

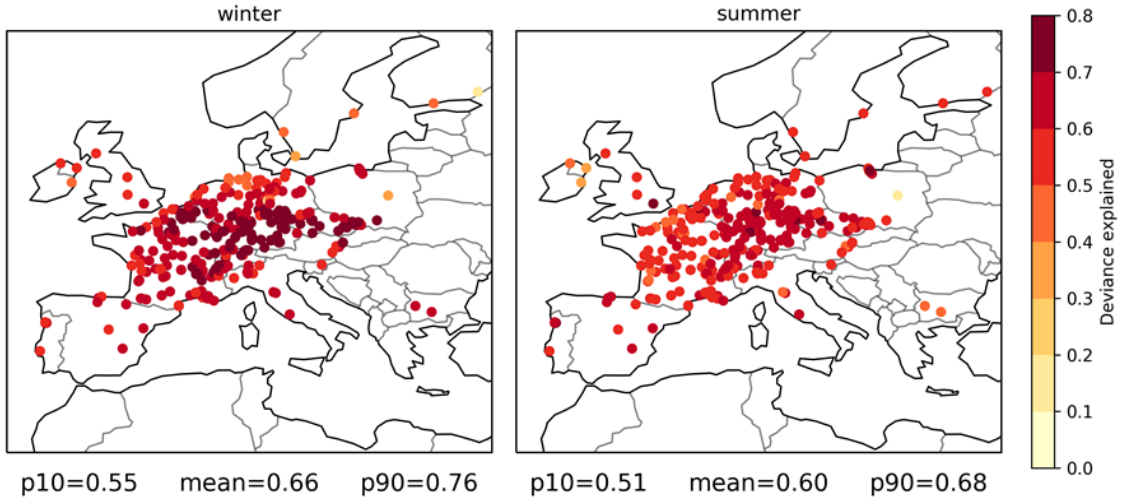

Figure 8. As Figure 7 but considering the persistence (defined as the mean PM_{10} concentration of the previous day), temperature and relative humidity as potential explanatory variables of PM_{10}.

While our analyses have proven the value of stagnation-related meteorological fields to identify conditions conducive to enhanced PM pollution, they also point to some potential limitations of the three ASIs evaluated here. These indices are based on fixed thresholds and cannot easily deal with non-linear relationships. In addition, ASIs disregard some relevant meteorological fields such as temperature and relative humidity. Consequently, statistical models based on the local selection of pollution-related variables might be more suited to reproduce the day-to-day variability of PM than ASIs. Nevertheless, it must be borne in mind that ASIs are qualitative indicators of air pollution potential and their usefulness goes beyond their ability to explain the variability of a specific air pollutant. In addition, the main advantages of these indices lie in their simplicity and in the fact that they often use common output variables that are provided by global and regional models (Horton et al., 2012; 2014; Caserini et al., 2017; Gao et al., 2020; Lee et al., 2020). This has clear implications for the long-term climatological assessment of air pollution potential. In this sense, the consideration of large-scale meteorological variables seems to be particularly relevant since future changes in regional climates are strongly driven by the atmospheric circulation (Woollings, 2010). Moreover, large-scale circulation anomalies generally arise as part of teleconnections linked to anomalies in other regions of the globe (e.g. Zappa and Shepherd, 2018). Therefore, special attention should be given to remote drivers of regional circulation and their impact on air pollution. For instance, recent studies have reported the influence of changes in Arctic sea ice and Eurasian snow cover on China's air pollution (Zou et al., 2017; Zhao et al., 2018; Kim et al., 2019), but these issues remain unexplored for Europe. The strong relationship between large-scale circulation and pollutant concentrations found in this and other studies (Garrido-Perez et al., 2017; Ordóñez et al., 2017, 2019) suggests that remote drivers might also play a key role in the long-term variability of air pollutant

concentrations in Europe. In particular, the tropical and Arctic amplification of global warming as well as changes in stratospheric vortex strength are potential candidates to be investigated in future work, since they shape different aspects of European climate such as precipitation and windiness, at least during the extended winter season (Zappa and Shepherd, 2018).

7. Conclusions

Recent studies have developed meteorological indices to identify stagnant conditions that favour the accumulation of pollutants in the lower atmospheric layers. Despite sharing common features, such air stagnation indices (ASIs) are defined based on different meteorological variables and their applicability may be geographically dependent. In this work, we have carried out a comparison of three ASIs (HO_ASI, Horton et al., 2012; HU_ASI, Huang et al., 2018; WA_ASI, Wang et al., 2018) to evaluate whether they capture the meteorological conditions conducive to elevated PM_{10} concentrations in Europe. For that purpose, we have used daily time series of 24-h average PM_{10} concentrations from the AirBase observational database together with ERA5 reanalysis data at 0.75º × 0.75º horizontal resolution. In addition, we have built generalized additive models (GAMs) to evaluate the complementarity of the different ASI components to reproduce the day-to-day variability of PM_{10}. The main findings are as follows:

- The application of the three ASIs results in similar spatial patterns of stagnation frequency, but also in important differences in the seasonal cycles. According to HO_ASI, the frequency of stagnation in Europe presents a summer maximum and a winter minimum, while the opposite is the case for HU_ASI. This occurs because HO_ASI uses predefined thresholds of wind speeds at 10 m and 500 hPa, whose values decrease in summer and increase in winter, whereas HU_ASI sets a threshold on the ventilation, which is higher in summer than in winter. On the other hand, the definition of WA_ASI considers different 10-m wind speed – boundary layer height conditions for each season, limiting the seasonal variability of this index.

- The response of the PM_{10} concentrations to stagnation varies with the ASI and also depends on the location and season. In winter, the application of the three ASIs yields similar positive PM_{10} anomalies (calculated as composite differences between the mean concentrations for stagnant and non-stagnant days), with averages over all sites ranging from 17.2 to 18.6 μg m^{-3}. In summer, the highest PM_{10} anomalies are found for HO_ASI over most of the area of study (on average 5.7 μg m^{-3}, considerably smaller than in winter). The main exceptions occur in coastal areas, where WA_ASI seems to be more powerful than the other ASIs.

- The consideration of the large-scale circulation consistently contributes to reproducing PM_{10} variability. Z500, SLP and wind speed at 500 hPa are among the most selected variables by the screening process used to find the best set of meteorological predictors. The selection frequency is especially high in summer, explaining the highest skill of HO_ASI during this season.

- Our results suggest that there is some room for improving the performance of HO_ASI and HU_ASI over Europe. This might require adapting the 500 hPa wind speed threshold to the season for the former and replacing the ventilation condition by an appropriate transport wind speed threshold in the latter.

- ASIs provide an incomplete description of the relationships between PM_{10} and meteorology. Since the three ASIs evaluated here are based on fixed thresholds, they cannot deal with non-linear relationships, which limits their ability to explain PM_{10} variability. In addition, PM_{10} concentrations also respond to changes in some meteorological fields such as temperature and relative humidity which are not indicators of stagnation.

Acknowledgments, Samples, and Data

This work was supported by the Spanish Ministerio de Educación, Cultura y Deporte [grant number FPU16/01972]; the Spanish Ministerio de Economía y Competitividad [grant number RYC-2014-15036]; and the Spanish Ministerio de Economía, Industria y Competitividad [grant numbers CGL2017-83198-R and RTI2018-096402-B-I00]. The authors are grateful to the European Environment Agency, the EU member states and collaborating countries for collecting and providing PM_{10} data through the Air-Base air quality database. ERA5 data are provided by ECMWF. We are also thankful to Mateusz Taszarek for helpful discussions on the calculation and use of CAPE and CIN in Europe. Three anonymous reviewers helped improve the original manuscript.

References

Aksoyoglu, S., Keller, J., Barmpadimos, I., Oderbolz, D., Lanz, V.A., Prévôt, A.S.H., Baltensperger, U., 2011. Aerosol modelling in Europe with a focus on Switzerland during summer and winter episodes. Atmos. Chem. Phys. 11, 7355–7373. https://doi.org/10.5194/acp-11-7355-2011

Anderson, J.O., Thundiyil, J.G., Stolbach, A., 2012. Clearing the Air: A Review of the Effects of Particulate Matter Air Pollution on Human Health. J. Med. Toxicol. 8, 166–175. https://doi.org/10.1007/s13181-011-0203-1

Barmpadimos, I., Hueglin, C., Keller, J., Henne, S., Prévôt, A.S.H., 2011. Influence of meteorology on PM_{10} trends and variability in Switzerland from 1991 to 2008. Atmos. Chem. Phys. 11, 1813–1835. https://doi.org/10.5194/acp-11-1813-2011

Barmpadimos, I., Keller, J., Oderbolz, D., Hueglin, C., Prévôt, A.S.H., 2012. One decade of parallel fine ($PM_{2.5}$) and coarse (PM_{10}-$PM_{2.5}$) particulate matter measurements in Europe: Trends and variability. Atmos. Chem. Phys. 12, 3189–3203. https://doi.org/10.5194/acp-12-3189-2012

Bencala, K.E., Seinfeld, J.H., 1976. On frequency distributions of air pollutant concentrations. Atmos. Environ. 10, 941–950. https://doi.org/10.1016/0004-6981(76)90200-6

Boleti, E., Hueglin, C., Takahama, S., 2018. Ozone time scale decomposition and trend assessment from surface observations in Switzerland, Atmos. Environ. 191, 440–451. https://doi.org/10.1016/j.atmosenv.2018.07.039

Cai, W., Li, K., Liao, H., Wang, H., Wu, L., 2017. Weather conditions conducive to Beijing severe haze more frequent under climate change. Nat. Clim. Chang. 7, 257–262. https://doi.org/10.1038/nclimate3249

Caserini, S., Giani, P., Cacciamani, C., Ozgen, S., Lonati, G., 2017. Influence of climate change on the frequency of daytime temperature inversions and stagnation events in the Po Valley: historical trend and future projections. Atmos. Res. 184, 15–23. https://doi.org/10.1016/j.atmosres.2016.09.018

Cohen, A.J., Brauer, M., Burnett, R., Anderson, H.R., Frostad, J., Estep, K., Balakrishnan, K., Brunekreef, B. Dandona, L., Feigin, V., Freedman, G., Hubbell, B., Jobling, A., Kan, H., Knibbs, L., Liu, Y., Martin, R., Morawska, L., Pope III, C.A., Shin, H., Straif, K., Shaddick, G., Thomas, M., van Dingenen, R., van Donkelaar, A., Vos, T., Murray C.J.L., Forouzanfar, M., 2017. Estimates and 25-year trends of the global burden of disease attributable to ambient air pollution: an analysis of data from the Global Burden of Diseases Study 2015. Lancet, 389(10082), 1907-1918. https://doi.org/10.1016/S0140-6736(17)30505-6

Dawson, J.P., Adams, P.J., Pandis, S.N., 2007. Sensitivity of $PM_{2.5}$ to climate in the Eastern US: A modeling case study. Atmos. Chem. Phys. 7, 4295–4309. https://doi.org/10.5194/acp-7-4295-2007

Dawson, J.P., Bloomer, B.J., Winner, D.A., Weaver, C.P., 2014. Understanding the meteorological drivers of U.S. particulate matter concentrations in a changing climate. Bull. Am. Meteorol. Soc. 95, 521–532. https://doi.org/10.1175/BAMS-D-12-00181.1

Dimitriou, K., 2015. The dependence of PM size distribution from meteorology and local-regional contributions, in Valencia (Spain) – A CWT model approach. Aerosol Air Qual. Res. 15, 1979–1989. https://doi.org/10.4209/aaqr.2015.03.0162

Dominici, F., McDermott, A., Zeger, S.L., Samet, J.M., 2002. On the use of generalized additive models in time-series studies of air pollution and health. Am. J. Epidemiol. 156, 193–203. https://doi.org/10.1093/aje/kwf062

European Environment Agency (EAA), 2019. Air quality in Europe – 2019 report. https://www.eea.europa.eu/publications/air-quality-in-europe-2019

EU, 2008. Directive 2008/50/EC of the European Parliament and of the Council of 21 May 2008 on ambient air quality and cleaner air for Europe. Official Journal of the European Union. OJ L 152, 11.6.2008, p. 1–44 https://eur-lex.europa.eu/legal-content/EN/TXT/PDF/?uri=CELEX:32008L0050&from=en

Feng, J., Quan, J., Liao, H., Li, Y., Zhao, X., 2018. An air stagnation index to qualify extreme haze events in northern China. J. Atmos. Sci. 75, 3489-3505. https://doi.org/10.1175/JAS-D-17-0354.1

Feng, J., Liao, H., Li, Y., Zhang, Z., Tang, Y, 2020. Long-term trends and variations in haze-related weather conditions in north China during 1980–2018 based on emission-weighted stagnation intensity. Atmos. Environ. 117830. https://doi.org/10.1016/j.atmosenv.2020.117830

Freund, R.J. and Wilson, W.J., 1998. Regression Analysis: Statistical modeling of a response variable. Academic Press, San Diego and London, 192 pp.

Friedman, J. H., 2001. Greedy Function Approximation: A Gradient Boosting Machine. Ann. Stat. 29: 1189–1232. https://doi.org/10.1214/aos/1013203451.

Fuzzi, S., Baltensperger, U., Carslaw, K., Decesari, S., Denier Van Der Gon, H., Facchini, M.C., Fowler, D., Koren, I., Langford, B., Lohmann, U., Nemitz, E., Pandis, S., Riipinen, I., Rudich, Y., Schaap, M., Slowik, J.G., Spracklen, D. V., Vignati, E., Wild, M., Williams, M., Gilardoni, S., 2015. Particulate matter, air quality and climate: Lessons learned and future needs. Atmos. Chem. Phys. 15, 8217–8299. https://doi.org/10.5194/acp-15-8217-2015

Gao, Y., Zhang, L., Zhang, G., Yan, F., Zhang, S., Sheng, L., Li, J., Wang, M., Wu, S., Fu, J.S., Yao, X., Gao, H., 2020. The climate impact on atmospheric stagnation and capability of stagnation indices in elucidating the haze events over North China Plain and Northeast China. Chemosphere 258, 127335. https://doi.org/10.1016/j.chemosphere.2020.127335

García-Herrera, R., Barriopedro, D., 2018: Climate of the Mediterranean Region. Oxford Research Encyclopedia of Climate Science. doi: 10.1093/acrefore/9780190228620.013.509. e-ISBN: 9780190228620.

Garrido-Perez, J.M., Ordóñez, C., García-Herrera, R., 2017. Strong signatures of high-latitude blocks and subtropical ridges in winter PM_{10} over Europe. Atmos. Environ. 167, 49–60. https://doi.org/10.1016/j.atmosenv.2017.08.004

Garrido-Perez, J.M., Ordóñez, C., García-Herrera, R., Barriopedro, D., 2018. Air stagnation in Europe: Spatiotemporal variability and impact on air quality. Sci. Total Environ. 645, 1238–1252. https://doi.org/10.1016/j.scitotenv.2018.07.238

Garrido-Perez, J.M., Ordóñez, C., García-Herrera, R., Schnell, J.L., 2019. The differing impact of air stagnation on summer ozone across Europe. Atmos. Environ. 219. https://doi.org/10.1016/j.atmosenv.2019.117062

Gietl, J.K., Klemm, O., 2009. Analysis of traffic and meteorology on airborne particulate matter in Münster, northwest Germany. J. Air Waste Manage. Assoc., 59(7), 809-818. https://doi.org/ 10.3155/1047-3289.59.7.809

Guerreiro, C.B.B., Foltescu, V., de Leeuw, F., 2014. Air quality status and trends in Europe. Atmos. Environ. 98, 376–384. https://doi.org/10.1016/j.atmosenv.2014.09.017

Heald, C.L., Henze, D.K., Horowitz, L.W., Feddema, J., Lamarque, J.F., Guenther, A., Hess, P.G., Vitt, F., Seinfeld, J.H., Godstein, A.H., Fung, I., 2008. Predicted change in global secondary organic aerosol concentrations in response to future climate, emissions, and land use change. J. Geophys. Res. Atmos. 113, 1–16. https://doi.org/10.1029/2007JD009092

[Dataset] Hersbach, H., Bell, B., Berrisford, P., Hirahara, S., Horányi, A., Muñoz-Sabater, J., Nicolas, J., Peubey, C., Radu, R., Schepers, D., Simmons, A., Soci, C., Abdalla, S., Abellan, X., Balsamo, G., Bechtold, P., Biavati, G., Bidlot, J., Bonavita, M., De Chiara, G., Dahlgren, P., Dee, D., Diamantakis, M., Dragani, R., Flemming, J., Forbes, R., Fuentes, M., Geer, A., Haimberger, L., Healy, S., Hogan, R.J., Hólm, E., Janisková, M., Keeley, S., Laloyaux, P., Lopez, P., Lupu, C., Radnoti, G., de Rosnay, P., Rozum, I., Vamborg, F., Villaume, S., Thépaut, J.N., 2020. The ERA5 global reanalysis. Q. J. R. Meteorol. Soc. 1–51. https://doi.org/10.1002/qj.3803

Horton, D.E., Harshvardhan, Diffenbaugh, N.S., 2012. Response of air stagnation frequency to anthropogenically enhanced radiative forcing. Environ. Res. Lett. 7, 044034. https://doi.org/10.1088/1748-9326/7/4/044034

Horton, D.E., Skinner, C.B., Singh, D., Diffenbaugh, N.S., 2014. Occurrence and persistence of future atmospheric stagnation events. Nat. Clim. Chang. 4, 698–703. https://doi.org/10.1038/nclimate2272

Huang, Q., Cai, X., Song, Y., Zhu, T., 2017. Air stagnation in China (1985–2014): climatological mean features and trends. Atmos. Chem. Phys. 17(12).

https://doi.org/10.5194/acp-17-7793-2017

Huang, Q., Cai, X., Wang, J., Song, Y., Zhu, T., 2018. Climatological study of the Boundary-layer air Stagnation Index for China and its relationship with air pollution. Atmos. Chem. Phys. 18, 7573–7593. https://doi.org/10.5194/acp-18-7573-2018

Hyslop, N.P., 2009. Impaired visibility: the air pollution people see. Atmos. Environ. 43, 182–195. https://doi.org/10.1016/j.atmosenv.2008.09.067

Jackson, L.S., Carslaw, N., Carslaw, D.C., Emmerson, K.M., 2009. Modelling trends in OH radical concentrations using generalized additive models. Atmos. Chem. Phys. Discuss. 8, 14607–14642. https://doi.org/10.5194/acpd-8-14607-2008

Jacob, D.J., Winner, D.A., 2009. Effect of climate change on air quality. Atmos. Environ. 43, 51–63. https://doi.org/10.1016/j.atmosenv.2008.09.051

Jiménez-Guerrero, P., Montávez, J.P., Gómez-Navarro, J.J., Jerez, S., Lorente-Plazas, R., 2012. Impacts of climate change on ground level gas-phase pollutants and aerosols in the Iberian Peninsula for the late XXI century. Atmos. Environ. 55, 483–495. https://doi.org/10.1016/j.atmosenv.2012.02.048

Kerr, G. H., Waugh, D. W., 2018. Connections between summer air pollution and stagnation. Environ. Res. Lett. 13(8). 084001. https://doi.org/10.1088/1748-9326/aad2e2

Kim, J.H., Kim, M.K., Ho, C.H., Park, R.J., Kim, M.J., Lim, J., Kim, S.J., Song, C.K., 2019. Possible link between Arctic Sea ice and January PM_{10} concentrations in South Korea. Atmosphere 10, 1–15. https://doi.org/10.3390/atmos10100619

Lecoeur, E., Seigneur, C., 2013. Dynamic evaluation of a multi-year model simulation of particulate matter concentrations over Europe. Atmos. Chem. Phys. 13, 4319–4337. https://doi.org/10.5194/acp-13-4319-2013

Lee, D., Wang, S.Y., Zhao, L., Kim, H.C., Kim, K., Yoon, J.H, 2020. Long-term increase in atmospheric stagnant conditions over northeast Asia and the role of greenhouse gases-driven warming. Atmos. Environ. 241, 117772. https://doi.org/10.1016/j.atmosenv.2020.117772

Liao, H., Chen, W.T., Seinfeld, J.H., 2006. Role of climate change in global predictions of future tropospheric ozone and aerosols. J. Geophys. Res. Atmos. 111, 1–18. https://doi.org/10.1029/2005JD006852

McClure, C.D., Jaffe, D.A., 2018. US particulate matter air quality improves except in wildfire-prone areas. Proc. Natl. Acad. Sci., 115(31), 7901-7906. https://doi.org/10.1073/pnas.1804353115

Mukherjee, A., Agrawal, M., 2017. World air particulate matter: sources, distribution and health effects. Environ. Chem. Lett. 15, 283–309. https://doi.org/10.1007/s10311-017-0611-9

Ordóñez, C., Barriopedro, D., García-Herrera, R., 2019. Role of the position of the North Atlantic jet in the variability and odds of extreme PM_{10} in Europe. Atmos. Environ. 210, 35-46. https://doi.org/10.1016/j.atmosenv.2019.04.045

Ordóñez, C., Barriopedro, D., García-Herrera, R., Sousa, P.M., Schnell, J.L., 2017. Regional responses of surface ozone in Europe to the location of high-latitude blocks

and subtropical ridges. Atmos. Chem. Phys. 17, 3111–3131. https://doi.org/10.5194/acp-17-3111-2017

Ordóñez, C., Garrido-Perez, J.M., García-Herrera, R., 2020. Early spring near-surface ozone in Europe during the COVID-19 shutdown: Meteorological effects outweigh emission changes. Sci. Total Environ. 747, 141322. https://doi.org/10.1016/j.scitotenv.2020.141322

Otero, N., Sillmann, J., Schnell, J.L., Rust, H.W., Butler, T., 2016. Synoptic and meteorological drivers of extreme ozone concentrations over Europe. Environ. Res. Lett 11, 024005. https://doi.org/10.1088/1748-9326/11/2/024005

Pateraki, S., Asimakopoulos, D.N., Flocas, H.A., Maggos, T., Vasilakos, C., 2012. The role of meteorology on different sized aerosol fractions (PM_{10}, $PM_{2.5}$, $PM_{2.5-10}$). Sci. Total Environ. 419, 124–135. https://doi.org/10.1016/j.scitotenv.2011.12.064

Putaud, J.P., Van Dingenen, R., Alastuey, A., Bauer, H., Birmili, W., Cyrys, J., Flentje, H., Fuzzi, S., Gehrig, R., Hansson, H.C., Harrison, R.M., Herrmann, H., Hitzenberger, R., Hüglin, C., Jones, A.M., Kasper-Giebl, A., Kiss, G., Kousa, A., Kuhlbusch, T.A.J., Löschau, G., Maenhaut, W., Molnar, A., Moreno, T., Pekkanen, J., Perrino, C., Pitz, M., Puxbaum, H., Querol, X., Rodriguez, S., Salma, I., Schwarz, J., Smolik, J., Schneider, J., Spindler, G., ten Brink, H., Tursic, J., Viana, M., Wiedensohler, A., Raes, F., 2010. A European aerosol phenomenology - 3: Physical and chemical characteristics of particulate matter from 60 rural, urban, and kerbside sites across Europe. Atmos. Environ. 44, 1308–1320. https://doi.org/10.1016/j.atmosenv.2009.12.011

REVIHAAP, 2013. Review of evidence on health aspects of air pollution - REVIHAAP Project. Technical Report. World Health Organization Regional Office for Europe. Bonn. http://www.euro.who.int/__data/assets/pdf_file/0004/193108/REVIHAAP-Final-technical-report-final-version.pdf

Servén D., Brummitt C., 2018. pyGAM: Generalized Additive Models in Python. Zenodo. https://doi.org/10.5281/zenodo.1208723

Sfetsos, A., Vlachogiannis, D., 2010. A new approach to discovering the causal relationship between meteorological patterns and PM_{10} exceedances. Atmos. Res. 98(2-4), 500-511. https://doi.org/10.1016/j.atmosres.2010.08.021

Tai, A.P.K., Mickley, L.J., Jacob, D.J., 2010. Correlations between fine particulate matter ($PM_{2.5}$) and meteorological variables in the United States: Implications for the sensitivity of $PM_{2.5}$ to climate change. Atmos. Environ. 44, 3976–3984. https://doi.org/10.1016/j.atmosenv.2010.06.060

Tai, A.P.K., Mickley, L.J., Jacob, D.J., Leibensperger, E.M., Zhang, L., Fisher, J.A., Pye, H.O.T., 2012: Meteorological modes of variability for fine particulate matter ($PM_{2.5}$) air quality in the United States: implications for $PM_{2.5}$ sensitivity to climate change, Atmos. Chem. Phys. 12, 3131–3145. https://doi.org/10.5194/acp-12-3131-2012

Taszarek, M., Brooks, H.E., Czernecki, B., Szuster, P., Fortuniak, K., 2018. Climatological aspects of convective parameters over Europe: A comparison of ERA-interim and sounding data. J. Clim. 31, 4281–4308. https://doi.org/10.1175/JCLI-D-17-0596.1

Vlachogianni, A., Kassomenos, P., Karppinen, A., Karakitsios, S., Kukkonen, J., 2011.

Evaluation of a multiple regression model for the forecasting of the concentrations of NO_x and PM_{10} in Athens and Helsinki. Sci. Total Environ. 409(8), 1559-1571. https://doi.org/10.1016/j.scitotenv.2010.12.040

Wang, J.X.L., Angell, J.K., 1999. Air stagnation climatology for the United States (1948-1998). Vol. 1. NOAA/Air Resources Laboratory ATLAS.

Wang, X., Dickinson, R.R.E., Su, L., Zhou, C., Wang, K., 2018. $PM_{2.5}$ pollution in China and how it has been exacerbated by terrain and meteorological conditions. Bull. Am. Meteorol. Soc. 99, 105–120. https://doi.org/10.1175/BAMS-D-16-0301.1

Wang, X., Wang, K., Su, L., 2016. Contribution of Atmospheric Diffusion Conditions to the Recent Improvement in Air Quality in China. Sci. Rep. 6, 1–11. https://doi.org/10.1038/srep36404

Wise, E.K., Comrie, A.C., 2005. Meteorologically adjusted urban air quality trends in the Southwestern United States. Atmos. Environ. 39, 2969–2980. https://doi.org/10.1016/j.atmosenv.2005.01.024

Wood, S.N., 2017. Generalized additive models: an introduction with R. Second ed. Chapman and Hall/CRC press. Boca Raton, USA, ISBN 9781498728331

Woollings, T., 2010. Dynamical influences on European climate: An uncertain future. Philos. Trans. R. Soc. A Math. Phys. Eng. Sci. 368, 3733–3756. https://doi.org/10.1098/rsta.2010.0040

Zappa, G., Shepherd, T.G., 2017. Storylines of atmospheric circulation change for European regional climate impact assessment. J. Clim. 30, 6561–6577. https://doi.org/10.1175/JCLI-D-16-0807.1

Zhao, S., Feng, T., Tie, X., Long, X., Li, G., Cao, J., Zhou, W., An, Z., 2018. Impact of Climate Change on Siberian High and Wintertime Air Pollution in China in Past Two Decades. Earth's Futur. 6, 118–133. https://doi.org/10.1002/2017EF000682

Zou, Y., Wang, Y., Zhang, Y., Koo, J.H., 2017. Arctic sea ice, Eurasia snow, and extreme winter haze in China. Sci. Adv. 3, 1–9. https://doi.org/10.1126/sciadv.1602751